ADVANCED FUNCTIONAL MATERIALS

FULL PAPER

DOI: 10.1002/adfm.200500529

Pharmacokinetics of Nanoscale Quantum Dots: In Vivo Distribution, Sequestration, and Clearance in the Rat**

By *Hans C. Fischer*, *Lichuan Liu*, *K. Sandy Pang*,* and *Warren C. W. Chan**

Advances in nanotechnology research on quantum dots (QDs)—water soluble ZnS-capped, CdSe fluorescent semiconductor nanocrystals—for in vivo biomedical applications have prompted a close scrutiny of the behavior of nanostructures in vivo. Data pertaining to pharmacokinetics and toxicity will undoubtedly assist in designing better in vivo nanostructure contrast agents or therapies. In vivo kinetics, clearance, and metabolism of semiconductor QDs are characterized following their intravenous dosing in Sprague–Dawley rats. The QDs coated with the organic molecule mercaptoundecanoic acid and crosslinked with lysine (denoted as QD-LM) are cleared from plasma with a clearance of 0.59 ± 0.16 mL min^{-1} kg^{-1}. A higher clearance (1.23 ± 0.22 mL min^{-1} kg^{-1}) exists when the QDs are conjugated to bovine serum albumin (denoted as QD-BSA, $P < .05$ (P = statistical significance). The biodistribution between these two QDs is also different. The liver takes up 40 % of the QD-LM dose and 99 % of QD-BSA dose after 90 min. Small amounts of both QDs appear in the spleen, kidney, and bone marrow. However, QDs are not detected in feces or urine for up to ten days after intravenous dosing.

1. Introduction

Recent breakthroughs in biomedical nanotechnology have demonstrated the promising clinical applicability of nanostructures as targeted diagnostic cancer-imaging agents,[1] as aids to optically guided surgery,[2] as smart drug-delivery systems,[3] and in hyperthermia therapy.[4] Of the existing biomedically applied nanotechnologies to date, CdSe-core, ZnS-capped semiconductor nanocrystals (also known as quantum dots, QDs) have been at the forefront of biomedical nanotechnology research.[5–7] Questions regarding the in vivo distribution, clearance, metabolism, and toxicity of the QDs have not been thoroughly investigated. Gao et al., Akerman et al., and Ballou et al. have provided the first qualitative glimpses of the in vivo distribution of QDs.[1,8,9] A thorough quantitative analysis of QD in vivo distribution and clearance is required, since this information could lead to i) an improvement in targeting efficiency of QDs for diagnostics, ii) a better understanding of QDs' non-specificity toward tissues, and iii) an assessment of QD distribution and clearance that serves as the basis in determining their toxicity. Therefore, the focus herein is to quantitatively elucidate the in vivo kinetics of QDs. We found that the modification of QDs' surface altered both the QD clearance from plasma and the sequestration of QDs within organs. Also, clearance of QDs via urine and feces was not observed within the experimental duration (ten days), suggesting that the QDs are sequestered in vivo and not cleared.

QDs are particles of dimensions that are smaller than the exciton Bohr radius. They generally have a core size of 2–7 nm, but can be as large as 100 nm when organic shells and/or conjugated biorecognition molecules are placed onto their surface. Recently, there has been interest in determining the in vivo toxicity of QDs, as in vivo exposure to QDs can lead to potential risks, which stem from three basic factors. The first involves the metallic component (e.g., Cd and Zn) of QDs, which are associated with known toxicity.[10,11] The second is due to the high surface-area-to-volume ratio of the QDs, which provides a large available surface for enzymatic degradation and release of metallic ions.[12] The third relates to the size of the QDs: it has been suggested that the small size of nanostructures, such as fullerenes, permits them to enter vital organs such as the brain and cause damage.[13]

Currently, no comprehensive study on the in vivo toxicity of QDs exists. Thus far, only in vitro cell-culture experiments on toxicity have been conducted. It has been shown that the breakdown of QDs can lead to metal-induced toxicity within the cells, and this toxicity is highly dependent on the chemical design of

[*] Dr. K. S. Pang, L. Liu
Leslie Dan Faculty of Pharmacy
University of Toronto
19 Russell St, Toronto, ON M5S 2S2 (Canada)
E-mail: ks.pang@utoronto.ca
Dr. W. C. W. Chan, H. C. Fischer
Institute of Biomaterials and Biomedical Engineering
University of Toronto
4 Taddle Creek Rd, Toronto, ON M5S 3G9 (Canada)
E-mail: warren.chan@utoronto.ca
Dr. W. C. W. Chan, H. C. Fischer
Department of Materials Science and Engineering
University of Toronto
184 College Street, Toronto, ON M5S 3E4 (Canada)

[**] W.C.W.C. and K.S.P. thank the CIHR (Novels Tools and NET grant), and NSERC (Discovery Grant and NanoIP), CFI, and OIT (W.C.W.C.) for research support. H.C.F. and L.L. were supported by the University of Toronto and OGS fellowships. We acknowledge Mr. Eli Papa for insightful discussions. We acknowledge the excellent assistance provided by the Analest Facility and Medical Sciences Electron Microscopy Facility.

the QD particles.[14,15] Although in vitro experimentation using cell-culture models provides some information on toxicity, quantitative in vivo kinetic studies are superior, since the results will assist in pinpointing the potential target organ and cells involved. For many pharmaceutical drug agents, quantitative pharmacokinetic studies in animals are the first step in determining drug dosing and toxicity; subsequently, based on the pharmacokinetic data, closer analysis on toxicity is then conducted on in vitro cell and tissue cultures. Ballou et al. conducted the first studies on QD in vivo kinetics by using whole-animal fluorescence imaging; their results provided a qualitative assessment of surface-chemistry-dependent kinetics of the QDs.[9] As a first step toward unraveling the question of whether or not QDs or engineered nanostructures are toxic in vivo, we quantitatively analyzed the fate (i.e., plasma-clearance studies, organ-uptake studies) of two chemically different QDs.

2. Results and Discussion

We studied the pharmacokinetics of QDs coated with mercaptoundecanoic acid (QD-LM) or bovine serum albumin (QD-BSA; see Fig. 1). The surface of QD-LM has a layer of lysine crosslinking, which exposes polar functional groups (i.e., carboxylic acid and amine) to the surrounding media.[16] This surface-modification strategy is typically used by commercial companies and research laboratories for preparing water-soluble QDs.[5,17–20] The conjugation of BSA to the surface of QD-LM creates QD-BSA. This provides a basis upon which to compare pre- and post-bioconjugated QDs. Fourier transform infrared (FTIR) spectroscopy was used to confirm the modifications with LM and BSA. Transmission electron microscopy (TEM) showed these water-soluble ZnS-capped, CdSe core QDs had a core size of 5.5 nm and were predominantly spherical, monodisperse, and free of agglomerations (Fig. 1A and B). The addition of an organic shell (mercaptoundecanoic acid with lysine crosslinking) increased the hydrodynamic diameter of the QDs from 7 to 25 nm, whereas conjugation to BSA yielded a hydrodynamic diameter of 80 nm. For further characterization details, see Jiang et al.[16] These values were determined using dynamic light scattering analysis (Malvern Particle Size Analyzer). To avoid interbatch variation, all experiments were conducted using the yield of one synthesis.

Methods to measure QDs in tissues were explored. The use of fluorescence to quantify the QD distribution in tissues was deemed problematic, owing to the high and variable background fluorescence from native blood and tissue. Moreover, the fluorescence of the QDs is susceptible to environmental factors—the quantum yield (unit brightness) has been demonstrated to change drastically with surface chemistry,[21] rearrangement of surface ligands,[22,23] photoenhanced oxidization,[24] and solvent effects.[25] Any of these would give rise to large error deviations in fluorescence measurements. Radiolabeling has been routinely employed to track injected species in pharmacokinetic studies, but the synthetic procedure and starting materials used in the syntheses of the QDs (e.g., dimethyl cadmium) render radiolabeling undesirable. Owing to these limitations, we used inductively coupled plasma atomic emission spectroscopy (ICP-AES) to measure the Cd concentration, which was correlated to the QD concentration.

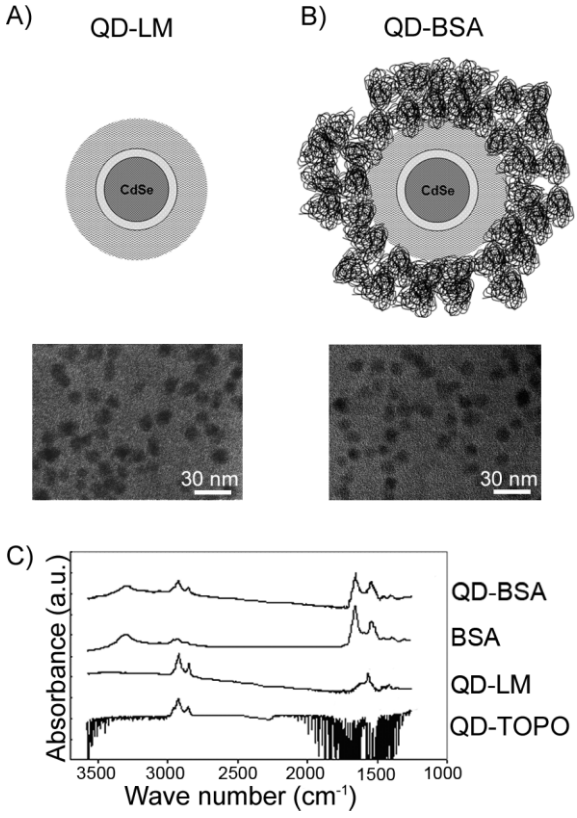

Figure 1. Nanoscale QDs used in this study. A) Schematic of CdSe core, as labeled, surrounded by ZnS capping. The surface of these QDs has an outer organic layer of mercaptoundecanoic acid crosslinked with lysine, and they are denoted as QD-LM. B) Schematic of the QD-LMs conjugated to BSA, denoted as QD-BSA. High-resolution transmission electron microscopy images of QD-LM and QD-BSA are also shown in (A) and (B), respectively. C) Comparative Fourier transform IR (FTIR) spectra of QDs to verify surface modification. In (C), QD-TOPO refers to QDs as synthesized: tri-octyl phosphine oxide-coated ZnS-capped CdSe.

Initially, we studied the plasma clearance of QDs to determine how fast the QDs leave the bloodstream and enter organs. We examined the decay of QDs in plasma as compared to that in whole blood. We verified with optical microscopy that QDs exhibited minimal, nonspecific binding to the cellular blood components of the rat (e.g., erythrocytes). After bolus injection of a 5 nmol dose of QDs into the jugular vein of the rat in vivo, the QD-LM and QD-BSA decayed monoexponentially in plasma according to first-order kinetics (Fig. 2). A dose of 5 nmol per rat (309 ± 53 g) is comparable to the reported dose for other in vivo QD experiments.[1,2,9]

From the ICP-AES analysis, the half-life for QD-LM ($t_{1/2(\mathrm{QD\text{-}LM})} = 58.5 \pm 17.0$ min) was significantly longer than that of QD-BSA ($t_{1/2(\mathrm{QD\text{-}BSA})} = 38.7 \pm 3.5$ min; $P < .05$ (P = statistical significance)). The half-life value was determined using the data from six animals. The volume of distribution (V), calculated as dose/concentration at zero time for QD-LM ($V_{\mathrm{QD\text{-}LM}} = 65.8 \pm 14.0$ mL kg^{-1}), was similar to that for QD-

ADVANCED FUNCTIONAL MATERIALS

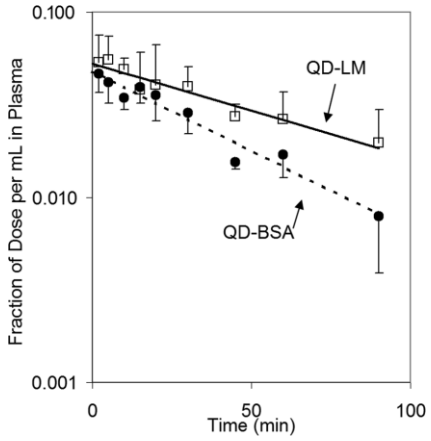

Figure 2. Plot of average data of QD-LM and QD-BSA concentrations vs. time after intravenous dosing of 5 nmol in the rat (mean ± standard deviation, number of animals, $n = 6$). The pharmacokinetic parameters (half-life, volume of distribution, and clearance) for each experiment were estimated individually and averaged to provide the mean data. The resulting half-life for QD-LM (□) was statistically longer than that for QD-BSA (●) (58.5 ± 17.0 vs. 38.7 ± 3.5 min, $P < .05$).

BSA ($V_{QD\text{-}BSA} = 67.9 \pm 10.9$ mL kg^{-1}; $P > .05$). The plasma clearance of the QD-LM ($CL_{QD\text{-}LM} = 0.84 \pm 0.30$ mL min^{-1} kg^{-1}), estimated as dose/area under the plasma concentration–time curve, was significantly lower than that for QD-BSA ($CL_{QD\text{-}BSA} = 1.22 \pm 0.20$ mL min^{-1} kg^{-1}; $P < .05$). The observed difference in the pharmacokinetics between QD-LM and QD-BSA likely stems from the described surface modification and the size of the QDs. However, further systemic investigations are required to understand the effect of surface chemistry and size on the pharmacokinetics of engineered nanostructures. Moreover, QDs are not ideal nanostructures for addressing these issues, because the surface charge and thickness of the organic shells of QDs (for different sizes) are difficult to manipulate and control. Therefore, we are currently using metallic nanostructures to investigate how these nanostructure parameters affect their in vivo kinetics.

Next, we examined the uptake of QDs into the various organs after leaving the bloodstream. Figure 3A and B show the organ-uptake curves of QDs. Previous studies reported on the accumulation of QDs in the liver and spleen using optical imaging, but these studies failed to show how much of the dose was taken up and at what rate.[9] Our results revealed that the majority of the QD dose was in the liver and not the spleen, even though the optical images of the QDs between the two tissues appeared similar. The much larger uptake of the liver versus the spleen is partially due to the much larger size of the liver, resulting in a higher fraction of dose sequestered. There was a big quantitative difference in tissue distribution between the QD-LM and QD-BSA in the liver, spleen, lung, and kidney. For example, 90 min after intravenous dosing, the accumulation of QD-LM (36.4 ± 8.1 % dose) in the liver was significantly lower than that of QD-BSA (99.5 ± 9.2 % dose; Fig. 3A and B). The spleen exhibited a much lower uptake of QD-LM (2.07 ± 0.43 % dose) and QD-BSA (2.19 ± 0.7 % dose; Fig. 3A and B) than the liver. The proportion of QD dose sequestered in the lymph nodes was even lower, and was undetected with ICP-AES (detection limit, 8 pmol g^{-1} tissue). However, the scant presence of QDs in the lymph nodes was observed by fluorescence imaging (Fig. 4). The bone marrow showed a higher accumulation of QD-BSA than QD-LM. A representative fluorescence image of QDs in bone marrow is shown in Figure 4.

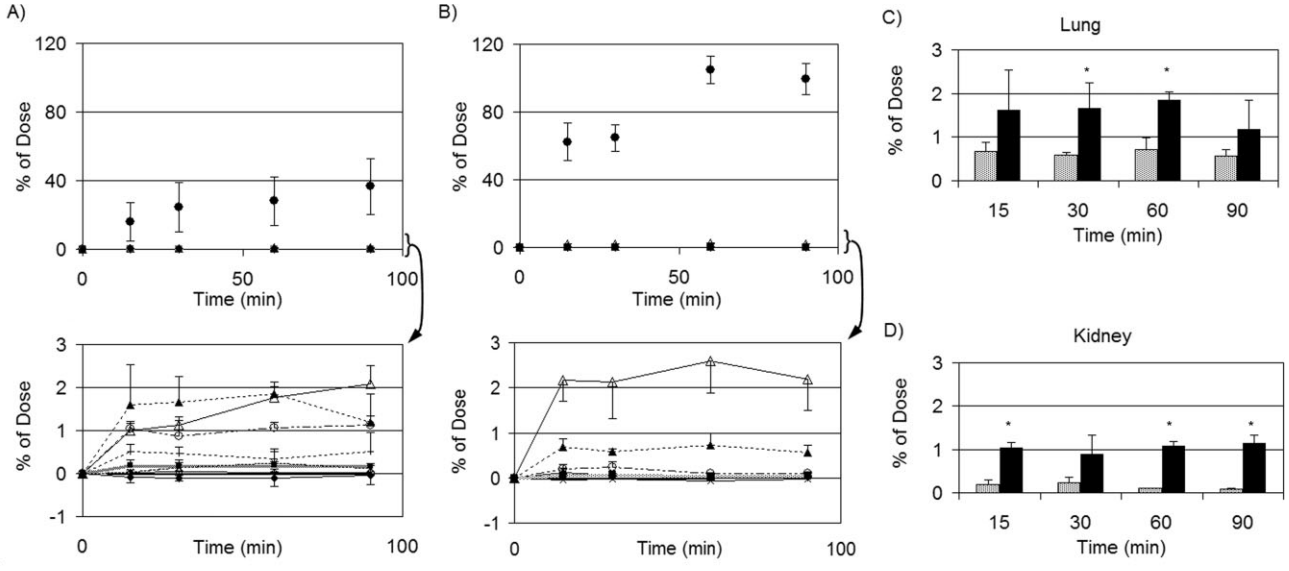

Figure 3. Organ distribution of QDs normalized to the intravenous dose (5 nmol), as measured by ICP-AES. A) QD-LM and B) QD-BSA nanoparticles were predominantly taken up by the liver (●). Accumulation of the QDs in other organs was much lower (spleen, △; lung, ▲; kidney, ○; colon, +; muscle, ×; brain, ◆; heart, ■; lymph node, –; bone marrow, ◇). C,D) A closer comparison further showed a greater uptake of QD-LM (solid black bar) than QD-BSA (solid gray bar) by the lung and kidney, respectively, suggesting that the uptake was dependent on surface modification ($n = 3$). The * denotes a significant difference between QD-LM and QD-BSA ($P < .05$).

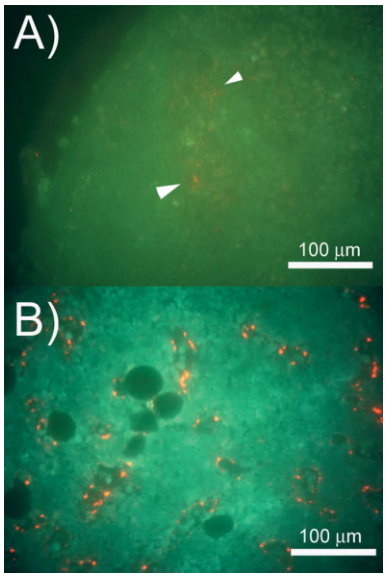

Figure 4. Representative fluorescence images of QD-BSA in A) the lymph nodes, and B) bone marrow 90 min after injection. The distribution of QD-LM in the lymph nodes and bone marrow is similar to that of QD-BSA. Both tissues were imaged with an Olympus IX71 inverted epi-fluorescence microscope, at 40× (numerical aperture, NA, 0.85). (Filters: $\lambda_{Excitation} = 360/40$ nm; $\lambda_{Emission} = 430$ nm long pass.)

A closer analysis of the fluorescence images of the liver shows localization of the QDs at the edges of the liver sinusoid (Fig. 5A–D). QDs were also localized in specific cells in the red pulp in spleen, within a small population of cells in the subcapsular sinus in the lymph nodes, and in the vascular sinus periphery in the bone marrow.

Furthermore, we want to highlight differences in the accumulation of QDs in the lung and kidney: QD-LM was present in higher quantities in both of these organs in comparison to QD-BSA (Fig. 3C and D). The sequestration of QD-LM in the lung was double that of QD-BSA (Fig. 3C), and for the kidney almost fourfold over that of QB-BSA (Fig. 3D). These results further confirm that molecules placed onto the surface of the QDs impact their pharmacokinetics and accumulation. These findings suggest that the elucidation of QD metabolism and clearance necessitate focused studies on the liver, kidney, and the reticuloendothelial system (RES).

TEM was used to identify cells that sequester QDs. We selected the liver for study; the rationale being that this organ contains the highest proportion of the QD dose and provides the best opportunity to locate the QDs within cells. The electron microscopy images showed that Kupffer cells took up the QDs and that the QDs appeared to enter the cells via phagocytic processes. Figure 5E and F both show that the QDs were trapped in vesicles in Kupffer cells. This observation suggests that the interaction of these nanostructures with the phagocytic cells is similar to the well-studied interaction between larger colloids and the RES.[26,27]

Our results suggest that the inorganic components of the QDs were not degraded within the short experimental duration in blood and tissue. The fact that the QDs retained their fluorescence in the tissues suggests that the QDs inorganic ZnS shells and CdSe cores are not degraded or metabolized. No conclusion on the integrity of the organic capping layer could be made from these results. Figure 5A–D clearly show the presence of bright fluorescence of the QDs in tissues. Ballou et al. also demonstrated that QDs maintained their fluorescence after several months in vivo.[9] Several groups have shown that the breakdown of the inorganic core/shell portion of the QDs, via photoexcitation or hydrogen peroxide oxidation, can lead to a decrease or loss of fluorescence from the QDs.[14,28] We used other techniques to verify that our conclusion on QD degradation is correct, since fluorescence may not be a dependable indicator of QD structural integrity. Hence, we explored further using TEM and a digestion–ultracentrifugation procedure. In the TEM images, the measured diameter of the QDs within Kupffer cell vesicles was similar to that of QDs prior to injection (Fig. 6).

We also conducted digestion–ultracentrifugation studies to verify that the ICP-AES measurements represented intact QDs in tissue. Homogenized spleen and liver tissues containing QDs 90 min post-injection were incubated in a sodium dodecylsulfate (SDS)–Proteinase K lysate buffer, and then ultracentrifuged at $500\,000 \times g$ for 105 min to provide the supernatant for analysis by ICP-AES. Cd, added to blank tissue, persisted in the supernatant after digestion and centrifugation. Cd would be absent in the supernatant obtained after digestion and centrifugation if the QDs remained intact in the tissue, and this absence was confirmed (Fig. 7). The measured Cd concentration from the spleen and liver tissues of rats dosed with 5 nmol of QDs failed to show signals above those of the blank tissues (which had no QDs; Fig. 7).

Feces and urine were collected and analyzed to determine if the QDs were cleared via the bile, intestinal lumen, or kidney. Surprisingly, measured levels of Cd excreted were not significantly different ($P > .05$) from background values of control rats, which received only the aqueous buffer phosphate buffered saline (Fig. 8). We therefore concluded that the QDs are sequestered and not excreted. Within the literature, there exist few studies on the excretion of nanoparticles. Renaud et al. showed that LDL-coated (LDL = low-density lipoprotein) 20 nm diameter gold nanoparticles entered hepatocytes and were excreted fecally, and further showed that the uptake of nanoparticles in hepatocytes was dependent upon the surface molecule on the nanoparticles.[29] In contrast, they showed that 20 nm BSA-coated gold nanoparticles were primarily taken up by Kupffer cells (similar to our results) and that they were not significantly excreted (0.07 % dose per day). As a result, they suggested that biliary excretion required hepatobiliary transport, which does not involve Kupffer cells. This leads one to conclude that nanoparticles taken up by Kupffer cells are not excreted via the fecal pathway. Renaud et al. suggest that if nanoparticles do excrete via the fecal pathway, it would be extremely slow, since nanoparticles may require degradation for efficient excretion. The elucidation of QD excretion mechanism and pathways will be important in the assessment of QD toxicity.

ADVANCED FUNCTIONAL MATERIALS

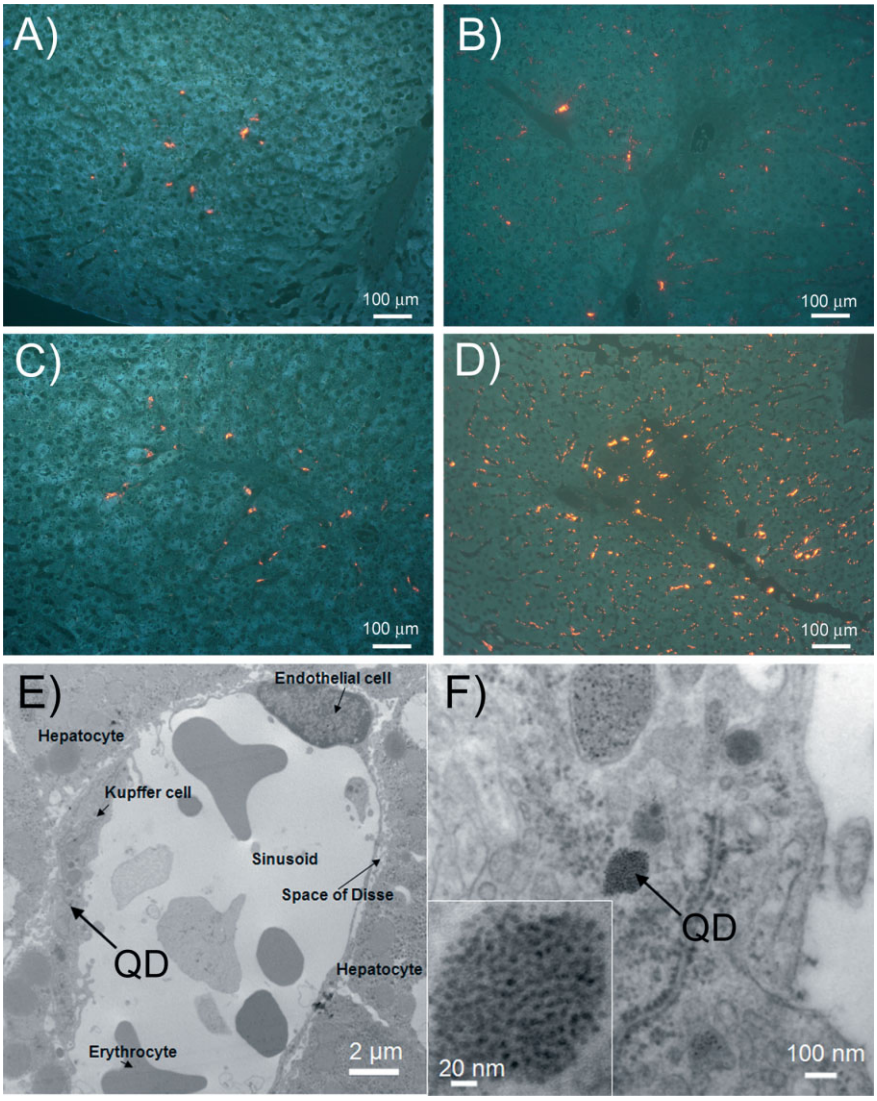

Figure 5. Optical fluorescence images showing accumulation of the QDs in the liver. Notably, the QD-LM at 30 min (A) shows less accumulation than QD-BSA at 30 min (B). At 90 min, both QD-LM (C) and QD-BSA (D) show an increased accumulation relative to the corresponding images at 30 min. Images A–D were generated with an Olympus IX71 inverted epifluorescence microscope, at 20× (NA 0.50). (Filters: $\lambda_{Excitation} = 350/50$ nm; $\lambda_{Emission} = 430$ nm long pass.) E) TEM image shows uptake in a Kupffer cell at the boundary of a hepatic sinusoid, and sequestration in phagosomes. The Kupffer cell can be identified by its active phagocytic surface morphology, and location within the sinusoid. F) A detailed microscopy image of the Kupffer cell shows QD accumulation in a cellular vesicle (inset is a high-magnification image of the QD agglomeration in the vesicle). For all fluorescence and TEM imaging, the tissue sections were prepared using standard histology techniques.

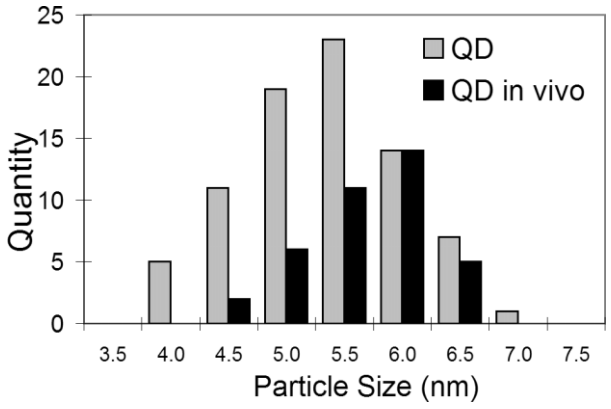

Figure 6. TEM comparison of pre- and post-injected QDs. The observed size distribution of the QDs sequestered in Kupffer cells (black) corresponds to the size distribution of the injected dose (gray). If the inorganic core/shell portion of the QDs had degraded, the black bars would be shifted to the left of the gray bars in the histogram. This was not observed. This data indicates the inorganic core/shell portion of the QDs is not degraded.

Ballou et al. have commented on the excretion of QDs.[9] By imaging and monitoring QDs in mice in vivo, they observed fluorescent signals arising from the intestine and concluded that the QDs were excreted in feces. In contrast, we directly assayed for QDs in feces and found that our results differed from that of Ballou et al. We did not observe any QDs in urine or feces. The difference may be due to the difference in coating chemistries between those used by Ballou et al. and those used in our study. There are currently over seven different commonly used QD surface coating chemistries; these surface chemistries are rapidly evolving (e.g., poly(ethylene glycol) surface coatings are commonly used for coating QDs for bioimaging) and will require further characterization.

3. Conclusions

We have estimated the in vivo pharmacokinetics and plasma clearance of QDs and their uptake by various organs, and identified the substructures of organs and cells that are responsible

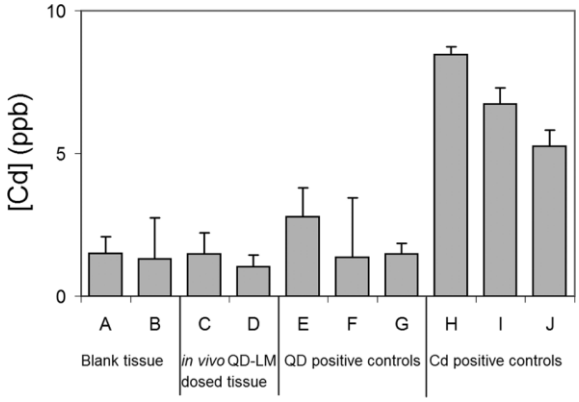

Figure 7. Digestion and ultracentrifugation studies to determine if ICP-AES measurements are derived from whole, intact inorganic core/shell QDs. We measured the ICP-AES signal of the supernatant after digestion and ultracentrifugation (500 000 × *g* for 105 min) of blank spleen (A) and liver (B) tissues; spleen (C) and liver (D) tissues obtained from intravenous QD-LM dosing; QDs in phosphate buffered saline, PBS (E); blank spleen (F), and liver (G) tissues spiked with QD-LM. Degradation of the QD would result in Cd in the supernatant after digestion and centrifugation; this was shown in the control samples in which an aqueous solution (H), blank spleen (I), and liver (J) tissues were spiked with Cd. In the above controls (E–G and H–J), equimolar concentrations of QD and Cd were used; these concentrations were also comparable to those obtained in the in vivo experiments. The absence of Cd in the spleen and liver samples (C,D) confirms the lack of degradation of the inorganic core/shell portion of the QDs.

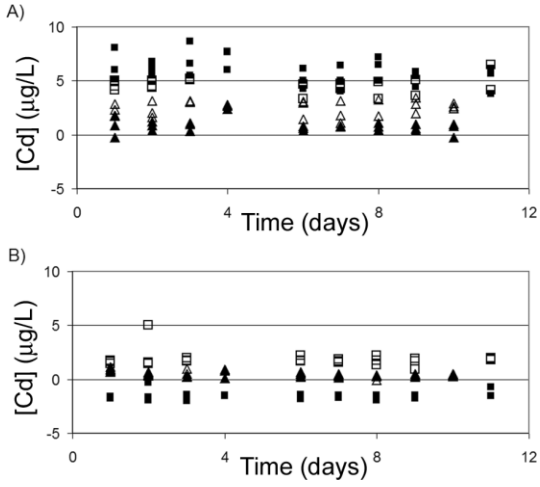

Figure 8. ICP-AES measurements of a) feces and b) urine of rats injected with QD-LM (■), QD-BSA (▲), or PBS (□ and △). Our results do not show any significant difference in the Cd level between experimental and control animals ($n = 3$).

for the sequestration of QDs. This is the first quantitative report on the biodistribution and clearance of QDs in vivo. Surprisingly, we failed to observe degradation of the inorganic core/shell part of the QDs, or excretion of the QDs in a short timeframe, but the QDs were sequestered in the RES cells. At this point, we speculate that the QDs may likely be re-distributed in vivo or resorbed at slow rates. Our quantitative findings are important for the advancement of QDs as contrast agents for cancer imaging, in terms of understanding the toxicity of QDs, and for improving the design of nanostructures for in vivo biomedical applications. This work provides a roadmap and general framework towards more focused studies for elucidating QD and nanostructure behavior in vivo.

4. Experimental

QD Synthesis: QDs were synthesized using established organometallic procedures [30]. We exchanged the surface of the QDs with mercaptoundecanoic acid and then crosslinked the surface with lysine, using dicyclohexylcarbodiimide to render the QD-LM water-soluble. We also conjugated the protein BSA on the surface of the QDs to yield QD-BSA, using 1-ethyl-3-(3-dimethylaminopropyl) carbodiimide. The resultant QDs were isolated and concentrated with the use of an Amicon column (Amicon, MWCO 100 kDa; 1 Da = 1.66×10^{-27} kg) prior to use in animal studies. The concentration was determined by measuring the absorbance of the QD solution, using the molar absorptivity coefficient reported by Peng and co-workers [31] according to Beer's law.

In Vitro Experiments: For investigation of whether the QDs interacted with blood components, QDs were incubated with whole blood, and samples were retrieved and centrifuged at various times. The supernatant (plasma) was analyzed for QDs using fluorescence spectroscopy and ICP-AES, whereas the pellet was further analyzed by fluorescence microscopy.

In Vivo Experiments: Male Sprague–Dawley rats (309 ± 53 g), obtained from Charles River Labs, St. Constant, QC, were given food and water ad libitum and housed in a 12 h/12 h light/dark cycle. Upon induction of anesthesia with pentobarbital (50 mg kg^{-1} given intraperitoneally), a midline incision of the neck region was made, and the jugular vein as well as the contralateral carotid artery were cannulated with PE-50 tubing and flushed with physiologic saline solution containing heparin (1000 IU (international units)).

Plasma Clearance: The QDs (5 nmol in a volume of 0.2 mL) were injected intravenously into the jugular vein cannula of the rat ($n = 6$ for each QD type), and blood samples (0.2 mL) were retrieved from the carotid artery at 2, 5, 10, 15, 20, 30, 60, and 90 min. The samples were immediately centrifuged to provide plasma. The kinetic parameters were estimated separately for each animal.

Organ-Uptake Studies: To characterize the biodistribution and accumulation of the QDs, the intravenous dose (5 nmol in a volume of 0.2 mL) was given as a bolus into the jugular vein ($n = 3$ for each time point, and each QD type). Animals were sacrificed under anesthesia at various times (0, 30, 60, and 90 min) by exsanguination. The abdomen was opened, the vena cava was ligated above the right renal vein, and ice-cold saline was perfused into the jugular cannula to remove blood that existed below the ligature at the vena cava. Additional saline solution was used for flushing until the organs become bleached of blood. Organs were then collected, blotted, and homogenized over ice in phosphate buffered saline (PBS; 10 mM, pH = 7.4) and prepared for ICP-AES analysis.

The liver, right kidney, spleen, descending colon, lumbar lymph nodes, leg muscle (parts of Vastus lateralis, Vastus Medialis, Rectus femoris), left femoral bone marrow, lungs, heart, and a central section of cerebellum were collected. Histological samples were carefully removed with a sharp razor blade and placed directly into fixative. Thereafter, tissues were excised and placed in pre-weighed centrifuge vials, weighed, and then kept on ice. PBS was added to the organ/tissue at a ratio of 3:1 (v/w). For the liver, a ratio of 2:1 buffer/liver was used. The tissues were homogenized and stored at –80 °C in 1 mL aliquots.

Optical microscopy was conducted on the excised, paraffin-embedded tissue samples, and these were de-waxed prior to observation. TEM sample preparation involved the use of electron-microscopy-grade fixative and embedding according to standard procedures. Uranyl acetate staining was applied only lightly to avoid obscuring the QDs or causing confusion with granular structures of similar sizes. Imaging was carried out on a Hitachi H-7000 transmission electron microscope, at 80 keV.

ADVANCED FUNCTIONAL MATERIALS

Metabolism studies were conducted by incubating 1 mL spleen and liver tissue homogenate (1:3 tissue to saline dilution) in lysate buffer (500 μL; 1 % SDS, 0.1 M NaCl, 0.05 M tris(hydroxymethyl)aminomethane, Tris, pH 8) and 25 μL Proteinase K (10 mg mL^{-1}) with the QDs overnight. After incubation, samples were diluted and placed into ultracentrifuge tubes (Beckman, Optiseal) for centrifugation at 500 000 × *g* for 105 min. Then 4 mL of the supernatant was carefully removed and digested for 2 h with 1 mL of HNO_3 in disposable glass culture tubes. ICP-AES analysis was then conducted to determine whether there was ionic cadmium in the tissue samples.

Excretion Studies: To address further whether the QDs were eliminated into urine or feces, rats ($n = 3$) were given tail-vein injections of QD-LM, QD-BSA (5 nmol in a volume of 0.2 mL), or saline (control) under sterile conditions, and were kept in Nalgene metabolic cages. Each animal was housed in a collection cage for 2 h every morning for ten days (11 days for QD-LM). Urine and feces were collected daily into pre-tared tubes, and the weight of the urine and feces were obtained by difference. Samples were refrigerated until analysis. For preparation of the fecal samples, a 3× excess weight of double-distilled water (DD-H_2O) was added to facilitate softening upon soaking for two days. Urine samples were diluted with an equal volume of DD-H_2O.

QD Concentration Analysis: ICP-AES was used to assay the QDs in the plasma, organ, and excretion samples. The samples were rendered soluble by the addition of reagent grade 70 % nitric acid. Samples, comprising of 50 μL of diluted plasma or 500 μL of tissue homogenate, were mixed with 0.5 mL or 1.0 mL of nitric acid, respectively. Urine samples were prepared by adding 1 mL of nitric acid to 0.5 mL of diluted urine. Fecal samples were prepared in a similar fashion, but 3 mL of nitric acid was used, since the sample contained more solid matter. All of the samples were prepared in disposable, 25 mL glass culture tubes that were fitted with polyethylene "snap caps". For all ICP-AES measurements, nitric acid blank, blank tissue samples, samples with QDs for calibration curves, and Cd standards were prepared and tested concurrently with test samples. With the cap punctured, acid digestion of the samples was carried out by heating in an oil bath at 110–120 °C for 2–3 h. Any remaining, undissolved solid was removed by passing the solution through a 0.45 μm pore poly(vinylidene fluoride) membrane syringe filter. The filtrate was re-diluted to 5 mL with DD-H_2O, and transferred to 15 mL polypropylene centrifuge tubes for storage prior to measurement. The concentrations of QDs in plasma, tissues, urine, and feces were determined by comparison to standard curves of QDs of known concentrations. We used optical absorbance to measure molar concentration [31], and analyzed standard solutions of known QD concentration with ICP-AES to provide a conversion from Cd [μg L^{-1}] to QDs [μmol mL^{-1}].

Received: August 10, 2005
Final version: November 23, 2005
Published online: June 12, 2006

[1] X. Gao, Y. Cui, R. M. Levenson, L. W. K. Chung, S. Nie, *Nat. Biotechnol.* **2004**, *22*, 969.
[2] S. Kim, Y. T. Lim, E. G. Soltesz, A. M. Degrand, J. Lee, A. Nakayama, J. A. Parker, T. Mihaljevic, R. G. Laurence, D. M. Dor, L. H. Cohn, M. G. Bawendi, J. V. Frangioni, *Nat. Biotechnol.* **2004**, *22*, 93.
[3] S. R. Sershen, S. L. Westcott, N. J. Halas, J. L. West, *J. Biomed. Mater. Res.* **2000**, *51*, 293.
[4] E. B. Voura, J. K. Jaiswal, H. Mattoussi, S. Simon, *Nat. Med.* **2004**, *10*, 993.
[5] W. Jiang, E. Papa, H. Fischer, S. Mardyani, W. C. W. Chan, *Trends Biotechnol.* **2004**, *22*, 607.
[6] I. L. Medintz, H. T. Uyeda, E. R. Goldman, H. Mattoussi, *Nat. Mater.* **2005**, *4*, 435.
[7] J. Riegler, T. Nann, *Anal. Bioanal. Chem.* **2004**, *379*, 913.
[8] M. E. Akerman, W. C. W. Chan, P. Laakkonen, S. N. Bhatia, E. Ruoslahti, *Proc. Natl. Acad. Sci. USA* **2002**, *99*, 12 617.
[9] B. Ballou, B. C. Lagerholm, L. A. Ernst, M. P. Bruchez, A. S. Waggoner, *Bioconjugate Chem.* **2004**, *15*, 79.
[10] K. Robards, P. Worsfold, *Analyst* **1991**, *116*, 549.
[11] G. J. Fosmire, *Am. J. Clin. Nutr.* **1990**, *51*, 225.
[12] *Nanoscience and Nanotechnologies: Opportunities and Uncertainties*, The Royal Society, Royal Academy of Engineering **2004**, Ch. 5.
[13] E. Oberdoerster, *Environ. Health Perspect* **2004**, *112*, 1058.
[14] A. M. Derfus, W. C. W. Chan, S. N. Bhatia, *Nano Lett.* **2004**, *4*, 11.
[15] C. Kirchner, T. Liedl, S. Kudera, T. Pellegrino, A. Munoz Javier, H. E. Gaub, S. Stolze, N. Fertig, W. J. Parak, *Nano Lett.* **2005**, *5*, 331.
[16] W. Jiang, S. Mardyani, H. Fischer, W. C. W. Chan, *Chem. Mater.* **2006**, *18*, 872.
[17] B. Dubertret, P. Skourides, D. J. Norris, V. Noireaux, A. H. Brivanlou, A. Libchaber, *Science* **2002**, *298*, 1759.
[18] X. Wu, H. Liu, J. Liu, K. N. Haley, J. A. Treadway, J. P. Larson, N. Ge, F. Peale, M. P. Bruchez, *Nat. Biotechnol.* **2003**, *21*, 41.
[19] S. Kim, M. G. Bawendi, *J. Am. Chem. Soc.* **2003**, *125*, 14 652.
[20] H. T. Uyeda, I. L. Medintz, J. K. Jaiswal, S. M. Simon, H. Mattoussi, *J. Am. Chem. Soc.* **2005**, *127*, 3870.
[21] C. Li, N. Murase, *Chem. Lett.* **2005**, *34*, 92.
[22] J. K. Lee, M. Kuno, M. G. Bawendi, *Mater. Res. Soc. Symp. Proc.* **1997**, 323.
[23] L. Xu, K. Chen, H. M. El-Khair, M. Li, X. Huang, *Appl. Surf. Sci.* **2001**, *172*, 84.
[24] N. Myung, Y. Bae, A. J. Bard, *Nano Lett.* **2003**, *3*, 747.
[25] K. Yu, B. Zaman, S. Singh, D. Wang, J. A. Ripmeester, *Chem. Mater.* **2005**, *17*, 2552.
[26] T. Saba, *Arch. Intern. Med.* **1970**, *126*, 1031.
[27] I. Carr, W. T. Daems, A. Lobo, in *The Reticuloendothelial System: A Comprehensive Treatise* (Eds: H. Friedman, M. Escobar, S. M. Reichard), Vol. 1, Plenum Press, New York **1980**.
[28] W. G. J. H. M. Van Sark, P. L. T. M. Frederix, D. J. Van Den Heuvel, H. C. Gerritsen, A. A. Bol, J. N. J. Van Lingen, C. De Mello Donega, A. Meijerink, *J. Phys. Chem. B.* **2001**, *105*, 8281.
[29] G. Renaud, R. L. Hamilton, R. J. Havel, *Hepatology* **1989**, *9*, 380.
[30] M. A. Hines, P. Guyot-Sionnest, *J. Phys. Chem. B* **1996**, *100*, 468.
[31] W. W. Yu, L. Qu, W. Guo, X. Peng, *Chem. Mater.* **2003**, *15*, 2854.

